Journal of Engineering Mathematics **26**: 87–106, 1992.
H.K. Kuiken and S.W. Rienstra (eds), Problems in Applied, Industrial and Engineering Mathematics.

Initial-value problems for spot disturbances in incompressible or compressible boundary layers

D.J. DOORLY[1] and F.T. SMITH*

*Department of Mathematics, University College London, Gower Street, London WC1E 6BT, UK (*author for correspondence); [1]current address: Department of Aeronautics, Imperial College, London SW7 2AZ, UK*

Abstract. This theoretical study of spot development in boundary layers is motivated by the need for some basic understanding of nonlinear spots, on which there appears to be little or no previous acceptable theory. The eventual aim is to be able to describe theoretically the transitional and/or turbulent spots which are often investigated experimentally. Here, as a starting point to guide possible nonlinear studies, we concentrate in particular on relatively long-scale inviscid spot disturbances in the context of the unsteady Euler equations, although short-scale with respect to Tollmien–Schlichting lengths for example. Both the incompressible and the compressible ranges are examined, for small disturbances, with the corresponding initial-value problems being treated computationally and analytically. The spatial spreading rate of the resulting spot is affected significantly by compressibility, and in fact tends to zero in the hypersonic extreme. The typical amplitudes provoked downstream and their decay lengths also vary considerably with the free-stream Mach number, producing two distinct structures in the transonic regime for example and an elongated structure in the hypersonic regime. The downstream behaviour found at comparatively large times, for finite Mach numbers, is used to provide guidance for nonlinear theory. There are also some potentially useful comparisons and links found with experiments, in both laminar and turbulent conditions.

1. Introduction

A 'spot disturbance' is the flow perturbation that develops from an initial disturbance, to a boundary layer in the present setting, with the typical development involving mostly downstream travel, some amplitude growth, and spatial spreading of the spot. The spot is a three-dimensional (3D) unsteady phenomenon, in general, and there would appear to be basically three types of spot, namely laminar, transitional and turbulent, depending on the amplitude and spectra of the initial disturbance. The three types have certain features in common, and others not. The two extremes of laminar and turbulent flow are studied experimentally and numerically in interesting works by Gaster & Grant (1975), Gaster (1975) and by Katz, Seifert & Wygnanski (1990), Riley & Gad-el-Hak (1985) (and references therein) for example, respectively, and many other experimental studies have also been made in the turbulent case, e.g. see additional references in the papers above and in Smith & Burggraf (1985) (SB), Smith, Doorly & Rothmayer (1990) (SDR), Gaster (1990). In the present work we start an attempt to theoretically understand the transitional and turbulent types of spot, in a compressible or incompressible boundary layer. Some simplification is necessary of course because such spots are very complex in practice, but the aim is to compare eventually with the experimental work above on such spots. While some previous studies of *ad hoc* linear theory have been made, little or no systematic theory/analysis has been done, as far as we know, especially on nonlinear initial-value problems relevant to transitional or turbulent spots, and on the scales and flow structures necessary for a clear physical understanding of the spots' behaviour. These aspects in fact provide the setting for the current study.

Concerning a systematic theory, and corresponding modelling, the 3D unsteady Euler

system (acting within the boundary layer) is believed to be very relevant to the transitional-turbulent regime: see SB, SDR, Walker & Smith (1991) and references therein. Thus SDR find agreement between Euler-stage theory and experiments on certain of the established scales for fully turbulent flow, pointing to the use of the Euler system coupled with an allowance for viscous sublayer bursting. The present investigation is therefore based on applying the 3D unsteady Euler system to the study of spot disturbances, this being related more to the transitional-turbulent regime than to the laminar one, and indeed we concentrate below on the inviscid dynamics of the initial-value problem for such spots.

The context for the spot-disturbance analysis is described in Section 2 below, first for an *incompressible* boundary layer (cf. the compressible case below) with an originally inflexion-free velocity profile. The main concern is with the 3D Euler setting, for the reasons mentioned above, and attention is then focussed on an unsteady 3D thin-layer version appropriate to relatively long-scale disturbances. In the thin-layer version the precise details of the original boundary-layer profile have negligible effect, apart from the $O(1)$ skin-friction factor (λ) and the local external velocity. The same version applies for the 3D unsteady triple-deck setting, which governs nonlinear Tollmien–Schlichting transitions (Smith 1989), provided relatively high-frequency disturbances are considered as described also in Section 2. These disturbances are relatively fast and have possible connections with some forms of by-pass transition (see in references above), although it should be observed that the high-frequency range tends to subjugate, or at least delay, the nonlinear break-up and possible intermittency described by Smith (1988), Peridier et al. (1991), Hoyle et al. (1991) for the complete 3D triple-deck system. Nevertheless, the break-up can still arise, as Peridier et al. show. We should add also that the response of a single or finite number of waves provoked by a maintained disturbance (e.g. as in Smith 1984, Smith & Stewart 1987a,b) is distinct from the present initial-value setting since here in effect all waves are activated. In Section 3, a linearized version is examined, as a first step, permitting a relatively simple analysis which produces useful and 'universal' results at large times, this representing an advantage over previous linear-disturbance studies, e.g. see references above and Ryzhov (1987), Smith (1987a). In particular, concentrated wake activity is found far downstream inside a wedge of half-angle $\sin^{-1}(1/3) = 19.47°$ (in plan view) and the maximum amplitude growth occurs at the edges of this wake (cf. the experiments of Wygnanski's group, e.g. Glezer, Katz & Wygnanski, 1989). This aspect is the same as for the Kelvin ship-wake (Whitham 1974), and as studied in another context by Cheng & Johnson (1982). The *compressible* boundary layer is then addressed in Section 4, yielding some very interesting changes in the spot development with increasing Mach number. These include especially the *transonic* range, where two main kinds of spot-disturbance amplitude response appear spatially, and the *hypersonic* range, in which the typical amplitudes produced are much reduced but last longer. The change in the wake half-angle mentioned above is also considered, as the Mach number increases, with the half-angle being found to tend to zero in the hypersonic range. Further comments are provided in Section 5, including suggestions for the nonlinear regime.

It is believed that the nonlinear 3D problems posed in Sections 2 and 4 could be very relevant to transitional and turbulent spot behaviour in practice, and further computations and analysis are desirable on these. The present first step, on the linear 3D regime, reveals certain interesting features of the incompressible and compressible initial-value problems, nevertheless, and in fact there are some signs that the experiments tie in qualitatively with the overall picture that emerges below, especially regarding the enhanced waviness in the

downstream wake. This tie-in is felt likely to increase once nonlinearity is accommodated. In the 2D case nonlinearity can lead to the Benjamin–Ono or Burgers equations (SB), after some simplification, and indeed the large-time scales found in Sections 3 and 4 agree with the scales associated with those equations, but in the more intriguing 3D case the nonlinear governing equations do not simplify so readily. The current work however enables estimates to be made (in Section 5) for the nonlinear 3D regime, studies of which are in progress (F.T.S.), while the results obtained below are also of potential practical value in gauging the spread of spots, following an initial disturbance in an incompressible or compressible boundary layer. There may be broader interest in addition with regard to the development of wavefronts.

The nondimensional velocity vector $\mathbf{u} \equiv (u, v, w)$ along with the corresponding Cartesian coordinates (x, y, z) (streamwise, normal, spanwise, respectively), the pressure p, and the time t, are used such that the typical free-stream velocity is $(1, 0, 0)$ and the undisturbed steady planar boundary layer has its x, y scales of order 1, $\mathrm{Re}^{-1/2}$ in turn, with a streamwise velocity profile written u_0. Here the global Reynolds number Re is taken to be large, for an incompressible (Sections 2 and 3) or compressible boundary layer (Section 4), and the 3D disturbance develops on length and time scales between $O(\mathrm{Re}^{-1/2})$ and $O(1)$. Some of the results from the present work are summarized and used in comparisons by Smith (1987a).

2. The two main contexts in 3D boundary-layer flow

There are two major areas in which the present work applies for boundary layers, (a), which is perhaps the more relevant to turbulent flow, and (b), which is more concerned with transition. These are addressed in turn below.

(a) The first concerns 3D unsteady Euler flow, in which the velocities and pressure are $O(1)$ but the spatial scales are all comparable with the boundary-layer thickness $O(\mathrm{Re}^{-1/2})$ and the corresponding time scale is then the convective one, $O(\mathrm{Re}^{-1/2})$. So the governing equations become

$$\boldsymbol{\nabla}\cdot\mathbf{u} = 0\,, \qquad \mathbf{u}_t + (\mathbf{u}\cdot\boldsymbol{\nabla})\mathbf{u} = -\boldsymbol{\nabla}p\,, \qquad \boldsymbol{\nabla} = (\partial_x, \partial_y, \partial_z)\,, \tag{2.1}$$

subject to appropriate boundedness conditions in the farfield including matching to the basic boundary-layer profile, $u = u_0(y)$ say upstream, and tangential flow $v = 0$ at $y = 0$. One solution is $\mathbf{u} \equiv (u_0, 0, 0)$ corresponding to undisturbed parallel motion, but linear and nonlinear waves are also possible and are of much interest. Nonlinear phenomena are especially important, in 2D or 3D (see SDR and references therein), giving possible connections with turbulence. Here we investigate long-scale 3D disturbances in particular, as suggested by Section 1, where a three-region structure arises analogous to that in (b) below. Thus $(x, z) = l(X, Z)$, say, with the length scale l being large, the main time scale has $t = l^2T$, where X, Z, T are typically $O(1)$, and three regions I–III appear in the y-direction, of scales l^{-1}, 1, l in which $y = l^{-1}Y$, y, $l\bar{y}$ and

$$[u, v, w, p] = \begin{cases} [l^{-1}U, l^{-3}V, l^{-1}W, l^{-2}P] + \cdots & \text{(2.2a)} \\ [u_0 + l^{-1}Au_0', -l^{-2}A_x u_0(y), l^{-2}D_1/u_0, l^{-2}P] + \cdots & \text{(2.2b)} \\ [1, 0, 0, 0] + l^{-2}[\bar{u}_2, \bar{v}_2, \bar{w}_2, \bar{p}_2] + \cdots & \text{(2.2c)} \end{cases}$$

in turn. Here P (the pressure), A (the negative displacement), D_1 are unknown functions of X, Z, T, with $D_{1X} \equiv -P_Z$. The small-disturbance expansion (2.2b) holding across most of the boundary layer satisfies (2.1) to the required order, whereas the near-wall response (2.2a) is controlled by the nonlinear unsteady thin-layer system

$$\bar{\nabla}\cdot\mathbf{U} = 0\,, \qquad \{\partial_T + \mathbf{U}\cdot\bar{\nabla}\}(U, W) = -(P_X, P_Z)\,, \quad \text{with } \bar{\nabla} \equiv (\partial_X, \partial_Y, \partial_Z) \tag{2.3a–c}$$

subject to

$$V = 0 \quad \text{at } Y = 0\,, \qquad U \sim \lambda(Y + A) \;\&\; W \to 0 \quad \text{as } Y \to \infty\,, \tag{2.3d}$$

from (2.1) and matching with (2.2b); and the outermost response (2.2c) leads from (2.1) to 3D quasi-steady potential-flow properties in the upper reaches of the boundary layer, so that $\bar{p}_2$ satisfies

$$(\partial_X^2 + \partial_{\bar{y}}^2 + \partial_Z^2)\bar{p}_2 = 0\,, \quad \text{with } \bar{p} \to P\,, \qquad \bar{p}_{2\bar{y}} \to A_{XX} \quad \text{as } \bar{y} \to 0\,, \tag{2.4a,b}$$

again to join to (2.2b), together with boundedness in the farfield. The solution of (2.4) therefore gives the relation

$$P(X, Z, T) = -\frac{1}{2\pi}\int_{-\infty}^{\infty}\int_{-\infty}^{\infty} \frac{A_{\xi\xi}(\xi, \eta, T)\,\mathrm{d}\xi\,\mathrm{d}\eta}{[(X-\xi)^2 + (Z-\eta)^2]^{1/2}}\,. \tag{2.5}$$

Hence we are left with solving the nonlinear problem (2.3) allied with the pressure-displacement law (2.5). We note in passing that the constant λ may be normalised to unity, the decay into the large-Y asymptote is algebraic, and a self-consistent initial condition is assumed at time $T = 0$.

(b) The second context is in 3D nonlinear triple-deck theory, which applies to the initial linear or nonlinear development of 3D TS waves and transition (Smith (1988, 1989) and references therein) and captures their viscous-inviscid nature. The governing equations here, mainly from the lower-deck flow where u, v, w, p, x, y, z, t are scaled with $\mathrm{Re}^{-m/8}$, $m = 1, 3, 1, 2, 3, 5, 3, 2$ respectively, are the 3D nonlinear boundary-layer equations

$$\nabla\cdot\mathbf{u} = 0\,, \qquad \{\partial_t + \mathbf{u}\cdot\nabla\}(u, w) = -(p_x, p_z) + \partial_y^2(u, w)\,, \tag{2.6a,b}$$

along with $p_y \equiv 0$, the constraints

$$\mathbf{u} = 0 \quad \text{at } y = 0\,, \qquad u \sim y + a \quad \text{and} \quad w \to 0 \quad \text{as } y \to \infty \tag{2.6c,d,e}$$

and the pressure-displacement law, which is given by (2.5) with the unknown functions $(p, a)(x, z, t)$ replacing (P, A) here. The basic inviscid problem (2.3), (2.5) therefore arises again if the viscous terms on the right in (2.6b) are simply neglected. More precisely, as in SB, for relatively high frequencies $|\partial_T| \sim \Omega \gg 1$ the scalings

$$\begin{aligned}&(u, v, w, p, a, x, y, z, t)\\ &\quad \sim (\Omega^{1/2}U, \Omega V, \Omega^{1/2}W, \Omega P, \Omega^{1/2}A, \Omega^{-1/2}X, \Omega^{1/2}Y, \Omega^{-1/2}Z, \Omega^{-1}T)\end{aligned} \tag{2.7}$$

lead to (2.3) coupled with (2.5).

In both of the contexts (a), (b) it should be emphasized that, as in 2D flow (SB, SDR), vorticity bursting is possible from the viscous sublayer assumed near the wall, in the nonlinear setting, although on the other hand bursting is not relevant in the linear regime studied subsequently. Further, in the special 2D case a simple solution of (2.3) is available, namely $U \equiv Y + A$, and the coupling with (2.5) thereby leads to the Benjamin–Ono equation for $A(X, T)$. Unfortunately no such simplification seems available in general in the full 3D case (Rothmayer & Smith 1987), and so (2.3), (2.5) as they stand, i.e. in terms of X, Y, Z, T, are in effect the 3D counterparts of the nonlinear Benjamin–Ono equation. The system (2.3), (2.5) is of much interest, then, in both contexts (a), (b) and as a start we concentrate next on one aspect of the system.

3. Development from an initial spot disturbance

Aspects of the travel, growth and spreading of an initial localised disturbance are considered in (i)–(iii) below.

(i) Linearized features hold for relatively small disturbances where the basic flow $U = Y$ is slightly disturbed. There to leading orders $(U - Y, V, W, P, A) = h(\hat{U}, \hat{V}, \hat{W}, \hat{P}, \hat{A})$, say, with $h \ll 1$, and so (2.3a–c) become

$$\nabla \cdot \hat{\mathbf{U}} = 0\,, \qquad \hat{U}_T + Y\hat{U}_X + \hat{V} = -\hat{P}_X,\ \hat{W}_T + Y\hat{W}_X = -\hat{P}_Z \tag{3.1a–c}$$

with $\hat{V} = 0$ at $Y = 0$, $\hat{U} \to \hat{A}$ and $\hat{W} \to 0$ as $Y \to \infty$, and (2.5) holds with $(\hat{P}, \hat{A})$ instead of (P, A). An appropriate solution may be derived from adding together the X-, Z-derivatives of (3.1b,c) respectively, which yields a quasi-2D system for $\hat{U}_X + \hat{W}_Z$, $\hat{V}_X$ whose solution, subject to suitable initial conditions, has $\hat{U}_X + \hat{W}_Z$ independent of Y and hence identically equal to $\hat{A}_X$. That is consistent with the momentum balances provided

$$\hat{A}_{XT} = -(\partial_X^2 + \partial_Z^2)\hat{P}\,. \tag{3.2}$$

Hence, combining this with (2.5), we obtain the equation

$$2\pi \hat{A}_{XT} = (\partial_X^2 + \partial_Z^2) \int_{-\infty}^{\infty} \int_{-\infty}^{\infty} \frac{\hat{A}_{\xi\xi}(\xi, \eta, T)\, \mathrm{d}\xi\, \mathrm{d}\eta}{[(X - \xi)^2 + (Z - \eta)^2]^{1/2}} \tag{3.3}$$

for $\hat{A}(X, Z, T)$, with a similar equation governing $\hat{P}$. Here (3.3) is a 3D extension of the 2D linearised Benjamin–Ono equation. We should remark that a benign critical layer is present in the $\hat{W}$ solution; see also later.

The solution of (3.3) may be found via a double Fourier transform (denoted **) in X, Z, which converts (3.3) to $\mathrm{i}\hat{A}_T^{**} = \alpha(\alpha^2 + \beta^2)^{1/2}\hat{A}^{**}$ where α, β are the transform variables corresponding to X, Z respectively. Hence

$$4\pi^2 \hat{A}(X, Z, T) = \int_{-\infty}^{\infty} \int_{-\infty}^{\infty} Q(\alpha, \beta) \exp\{\mathrm{i}\alpha X + \mathrm{i}\beta Z - \mathrm{i}\alpha(\alpha^2 + \beta^2)^{1/2} T\}\, \mathrm{d}\alpha\, \mathrm{d}\beta \tag{3.4}$$

where $Q(\alpha, \beta)$ is the initial distribution of the negative displacement transform, $A^{**}(\alpha, \beta, 0)$. Here (3.4) determines the development of the displacement in space and time,

and hence the pressure from (2.5), for any prescribed initial distribution. We note that (3.4) agrees with the dispersion relation obtained in allied previous papers, although the flow structure shown above in the derivation of (3.4) is worth emphasising, as discussed later. It is apparent also that the dispersion relation involved yields only neutral waves in the present regime.

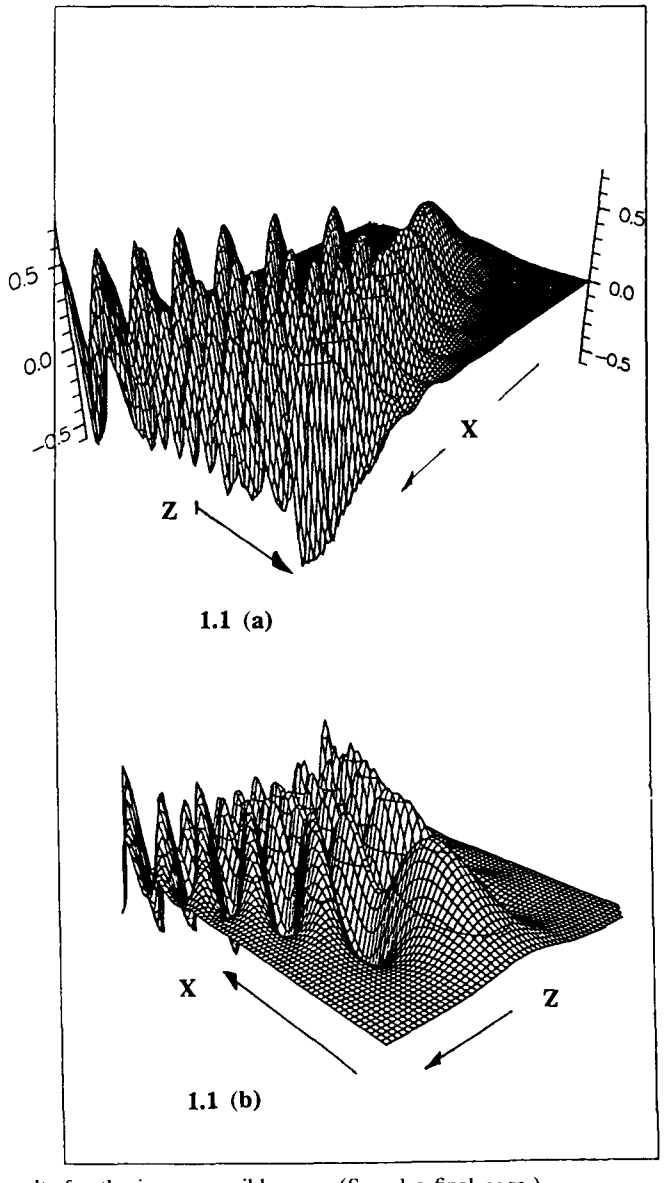

Fig. 1. Numerical results for the incompressible case. (See also final page.)

1.1. (a)(b) Surface plots of disturbance $\hat{A}(\bar{X}, \bar{Z}, T)$ for very large time T. ($T = 256$)

1.2. (a)(b) Surface plot of $\hat{A}(\bar{X}, \bar{Z}, T)$ for short time T. ($T = 2$)

1.3. (a) Contour plot of $\hat{A}(\bar{X}, \bar{Z}, T)$ for short (a) and large time (b). (Results symmetric about $\bar{Z} = 0$. At large times, the maximum amplitudes are clearly seen to lie along the caustic.)

1.4. (a) Centreline amplitudes for various values of time T.

(b) Amplitudes along caustic at various values of T.

1.5. Amplitude growth along caustic. Theoretical slope = $\frac{1}{3}$ (since $\hat{A} \sim O(r^{1/3})$), computational slope = 0.3.

(ii) Computations of (3.4) were performed for a number of different initial conditions, by use of a spectral scheme. Sample results are shown in Fig. 1.

(iii) Of special interest now is the behaviour of the flow solution at large times, for $O(1)$ or large distances from the start. There (3.4) suggests that significant effects arise mainly in two regions far downstream, the first of which has X, Z large and $O(T^{1/2})$, say $(X, Z) = T^{1/2}(\bar{X}, \bar{Z}) = T^{1/2}R(\cos\theta, \sin\theta)$. There, in (3.4), $(\alpha, \beta) = T^{-1/2}(\bar{\alpha}, \bar{\beta}) = T^{-1/2}\bar{r}(\cos\phi, \sin\phi)$ in polars, yielding

$$2\pi\hat{A} \sim T^{-1}Q(0,0)\int_0^\infty \bar{r}J_0(\Phi)\,\mathrm{d}\bar{r} \quad \text{with } \Phi^2 = \bar{r}^2R^2 - 2\bar{r}^3R\cos\theta + \bar{r}^4\,, \tag{3.5}$$

after a ϕ-integration, where J_0 is the standard Bessel function of zeroth order. Here (3.5) gives most of the large-time behaviour for $O(1)$ values of the scaled distance $R \equiv$

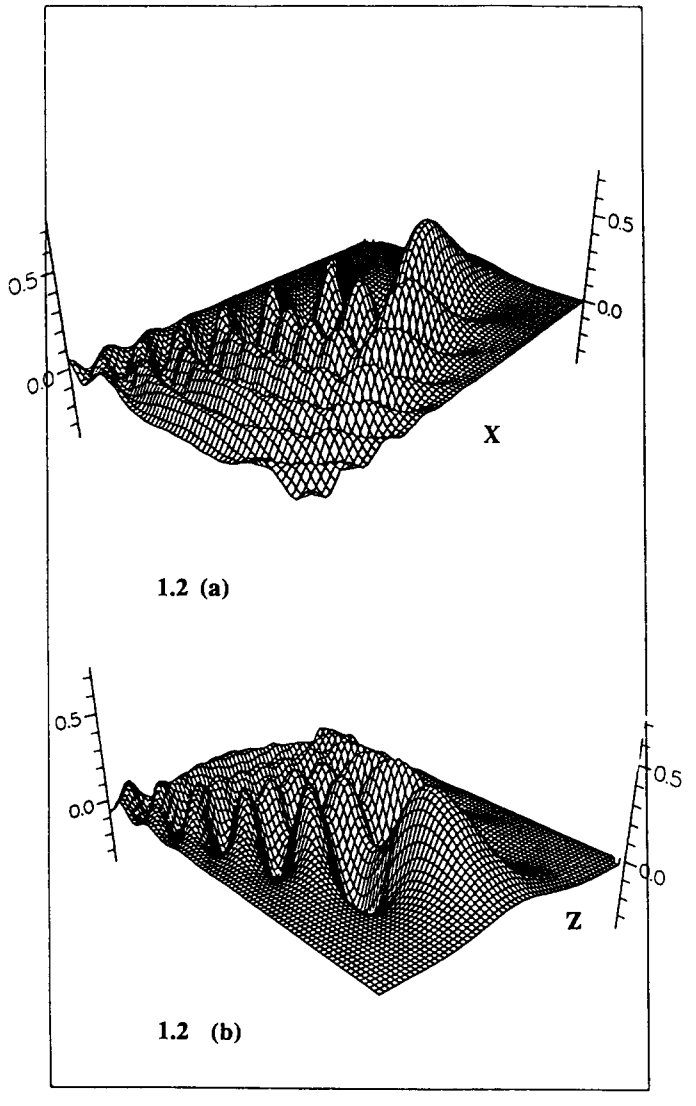

Fig. 1 (cont.).

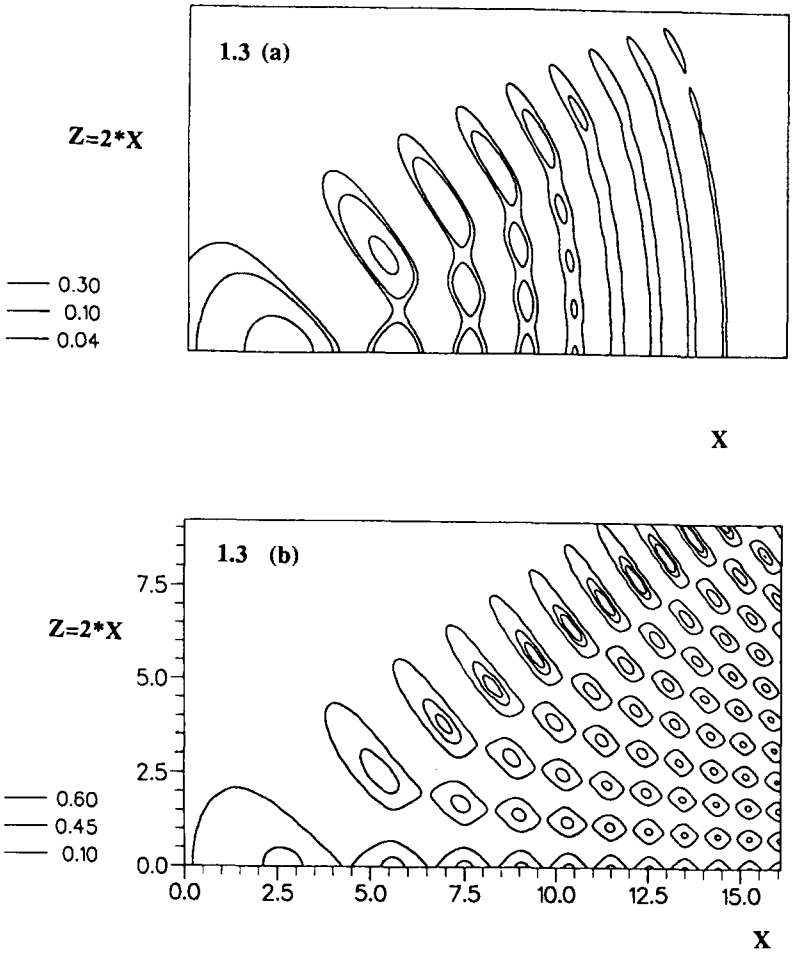

Fig. 1 (cont.).

$(X^2 + Z^2)^{1/2}T^{-1/2}$ and angles θ. The constant $Q(0, 0)$ is an integral property of the initial displacement, specifically the double integral with respect to X, Z of the initial disturbance $A(X, Z, 0)$. For *smaller* R values, the range $\bar{r} \sim 1$ dominates, giving

$$\hat{A} \sim T^{-1}Q(0,0)\{c_1 + c_2T^{-1/2}X + O(T^{-1})\} \text{ [for } R \ll 1] \tag{3.6}$$

where c_1, c_2 are constants, whereas for *larger* distances R the beginning of a confined 'wake' can be distinguished. For then the range $\bar{r} = \sigma R \gg 1$ matters, giving $\Phi^2 = R^4(\sigma^2 - 2\sigma^3 c + \sigma^4) \gg 1$ [where $c = \cos\theta$] and so $J_0(\Phi) \sim (2/\pi\Phi)^{1/2}\cos(\Phi - \pi/4)$. The major effects therefore come from the maxima of $h(\sigma) \equiv (\sigma^2 - 2\sigma^3 c + \sigma^4)$, since J_0 is predominantly oscillatory. But $h'(\sigma) = 2\sigma\{2(\sigma - 3c/4)^2 + (1 - 9c^2/8)\}$. So the maxima are possible only for $c^2 > 8/9$, i.e. at angles $|\theta| < \theta_s$ where

$$\theta_s = \sin^{-1}\left(\frac{1}{3}\right) = 19.47^\circ . \tag{3.7}$$

For such angles, (3.5) then gives the asymptote

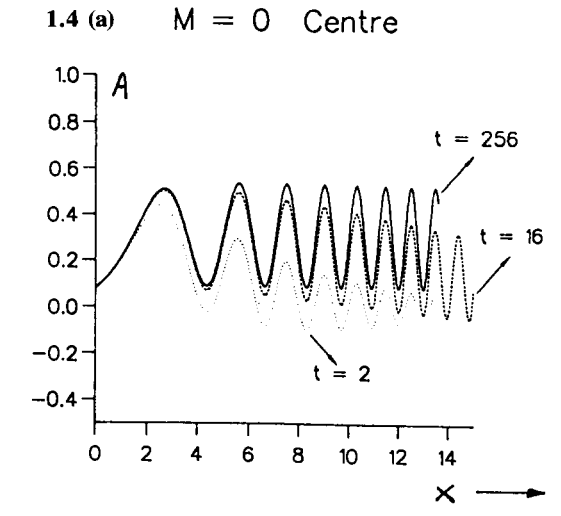
1.4 (a) M = 0 Centre
A
t = 256
t = 16
t = 2
x

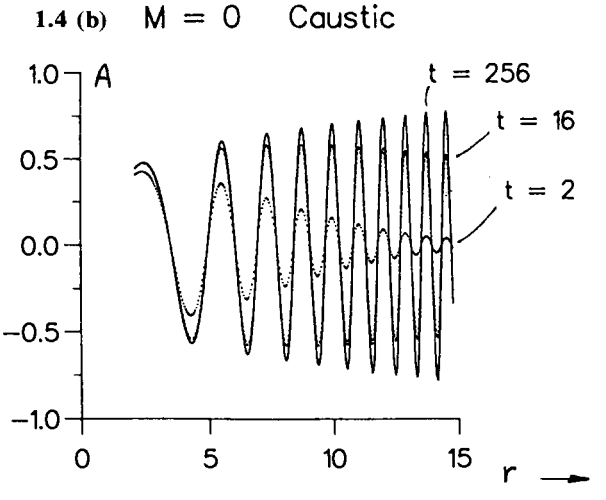
1.4 (b) M = 0 Caustic
A
t = 256
t = 16
t = 2
r

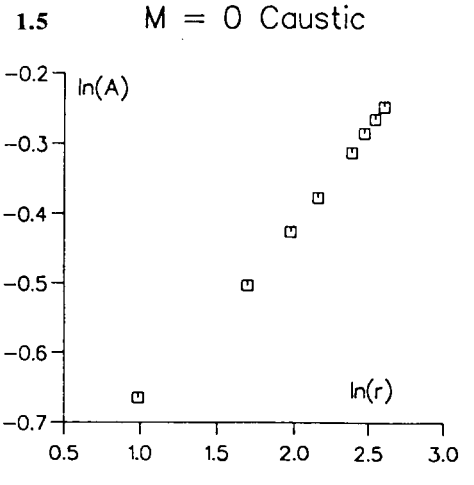
1.5 M = 0 Caustic
ln(A)
ln(r)

Fig. 1 (cont.).

$$2^{1/2}\pi\hat{A} \sim T^{-1}Q(0,0)\left[\frac{\sigma_1^+}{(B_1^+B_2^+)^{1/2}}\cos(R^2B_1^+) + \frac{\sigma_1^-}{(B_1^-B_2^-)^{1/2}}\cos(R^2B_1^-)\right],$$

$$\text{for } R \gg 1 \text{ with } -\theta_s < \theta < \theta_s\,, \tag{3.8a}$$

consisting of two wave forms in which

$$B_1(\theta) = (\sigma_1^2 - 2\sigma_1^3 c + \sigma_1^4)^{1/2}\,, \tag{3.8b}$$

$$B_2(\theta) = \frac{1}{2}(1 - 6\sigma_1 c + 6\sigma_1^2)B_1^{-1}\,, \qquad \sigma_1^{\pm}(\theta) = \frac{1}{4}\{3c \pm (9c^2 - 8)^{1/2}\}\,. \tag{3.8c,d}$$

From this it can be seen that increasingly concentrated (i.e. relatively short-wavelength) waves form in the wake far downstream, with their maximum amplitudes occurring at the *edges* $\theta \sim \pm\theta_s$, since $B_2 \to 0$, $B_1 \to O(1)$ as $|\theta| \to \theta_s^-$. Near each edge (or caustic), a relatively thin layer is present in which $\hat{A}$ acquires the form of an Airy function, matching with (3.8a) inside the wake and with the exponentially small response outside (for $|\theta| > \theta_s$). In detail, (3.5) gives

$$2\pi\hat{A} \sim \left(\frac{8\pi}{B_1}\right)^{1/2}\sigma_1\left(\frac{2}{a}\right)^{1/3}R^{1/3}\cos(B_1R^2)Ai(\eta)\,, \quad \text{for } R \gg 1 \text{ near } \theta = \theta_s\,, \tag{3.9}$$

where $\eta \equiv 2^{1/2}\bar{X}^{4/3}3^{-1/3}(\bar{Z}/\bar{X} - 8^{-1/2})$ is $O(1)$ in the edge layer and now $\sigma_1 = 3c/4$, $B_1 = 3^{-1/2}/2$, $c = 3^{-1}2^{3/2}$, $\bar{X} = cR$, $a = 2^{5/2}3^{1/2}$.

The second region, further downstream, occurs where the distances X, Z are increased to $O(T)$, cf. Figs 1.3, 1.4 and below. There, in view of (3.5)ff, the major contributions to the integral (3.4) come from $O(1)$ values of α, β. So the new feature emerging here is that the detailed distribution $Q(\alpha, \beta)$ now modifies the solution amplitude at leading order, i.e. this region feels the 'footprint' of the initial disturbance $\hat{A}(X, Z, 0)$. There are again two wave families present containing an infinite number of waves analogous with those in (3.8a) but the typical wavelength is reduced to $O(1)$. Moreover, the wake remains confined to $|\theta| < \theta_s$,

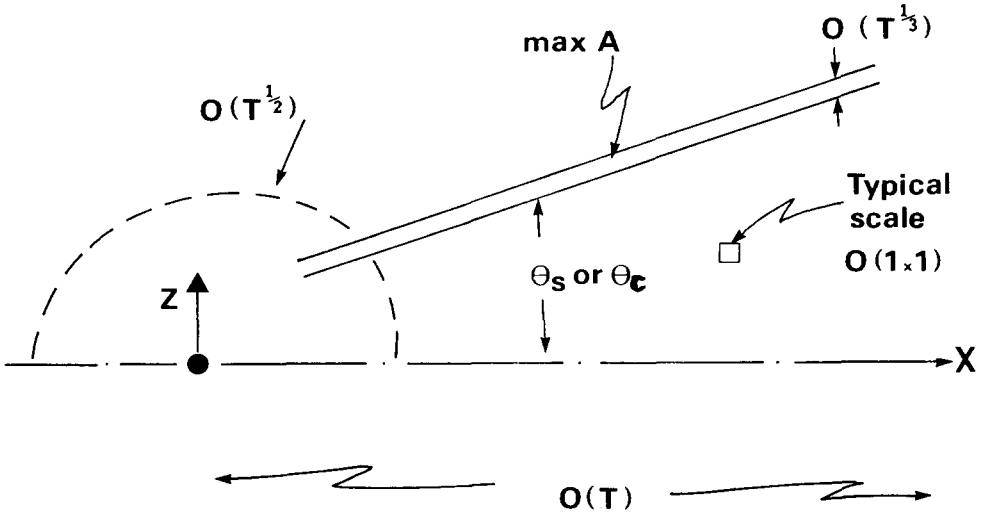

Fig. 2. Sketch of the structure for the large-time large-distance behaviour. Plan view: upper half only.

with a modified form of (3.9) applying in an edge region of thickness $O(T^{1/3})$ in terms of $Z - 8^{-1/2}X$. The final downstream decay of the solution is then obtained at distances greater than $O(T)$.

The analytical features here, summarized in Fig. 2, are also well brought out in the computed results of Fig. 1, and there is broad agreement in fact with the computational trends obtained in (ii) above. We refer in particular to Figs 1.4a, 1.4b concerning the centre-line and the near-caustic calculations, as time T increases, and note that the slope of the log–log plot in Fig. 1.5 at large distances is very close to $\frac{1}{3}$, cf. (3.9).

4. The compressible regime

Most of the reasoning in Section 2 for the 3D nonlinearly disturbed incompressible boundary layer can be adapted also for the compressible case studied next. Thus, from scaling of the unsteady compressible Euler equations, (2.3a–d) still hold, but the outer potential-flow part in (2.4a,b) or (2.5) must be replaced by

$$(M_\infty^2 - 1)(\bar{p}_{2XX} \pm \bar{p}_{2\bar{y}\bar{y}}) - \bar{p}_{2ZZ} = 0 \tag{4.1a,b}$$

(e.g. as in Smith 1989), along with (2.4b), for the subsonic ($0 \leqslant M_\infty < 1$) and supersonic ($M_\infty > 1$) ranges respectively, where M_∞ is the Mach number. [Shorter-scale contributions are omitted; see Section 5]. In consequence the linearized properties replacing those of Section 3 are as follows, for the development from an initial spot disturbance.

In the *subsonic* regime, (4.1a) leads to the result

$$4\pi^2 \hat{A}(X, Z, T) = \int_{-\infty}^{\infty} \int_{-\infty}^{\infty} Q(\alpha, \beta) \exp\left\{ i\alpha X + i\beta Z - \frac{i\alpha(\alpha^2 + \beta^2)T}{(\alpha^2 + \kappa^2\beta^2)^{1/2}} \right\} d\alpha \, d\beta \tag{4.2}$$

for the negative displacement, with $\kappa \equiv (1 - M_\infty^2)^{-1/2}$ ranging from 1 to ∞. Spectral computations for (4.2) were performed as in Section 3(ii) at several subsonic Mach numbers, giving the results shown in Fig. 3. Analytically, rather than proceeding as in Section 3(iii) we may use the method of stationary phase to deduce the large-time behaviour, setting $(X, Z) = T^{1/2}R(\cos\theta, \sin\theta)$, $(\alpha, \beta) = T^{-1/2}\bar{r}(\cos\phi, \sin\phi)$ again and then $\bar{r} = \sigma R$, to convert (4.2) to the form

$$4\pi^2 \hat{A} \sim Q(0,0) T^{-1} R^2 \int_0^{\infty} \int_0^{2\pi} \exp\left\{ i\left[\sigma \cos(\phi - \theta) - \sigma^2 \frac{\cos\phi}{K(\phi)} \right] R^2 \right\} \sigma \, d\sigma \, d\phi \tag{4.3a}$$

for large distances R, where

$$K(\phi) \equiv (\cos^2\phi + \kappa^2 \sin^2\phi)^{1/2} . \tag{4.3b}$$

The maximum contributions to $\hat{A}$ at large R therefore come from the extrema of the expression in square brackets in (4.3a). With the derivatives of that expression, with respect to σ, ϕ, equated to zero, then, we obtain two equations to determine the extremal values of σ, ϕ, leading to the equation

$$\kappa^2\chi^4 \tan\theta - \kappa^2\chi^3 + 3\kappa^2\chi^2 \tan\theta + (\kappa^2 - 2)\chi + 2\tan\theta = 0 \tag{4.4}$$

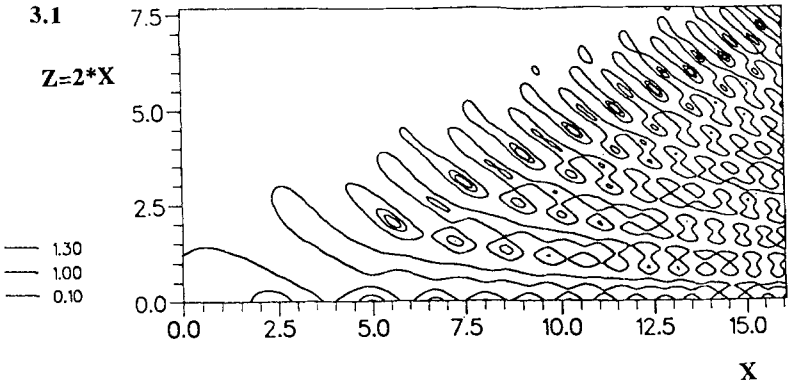

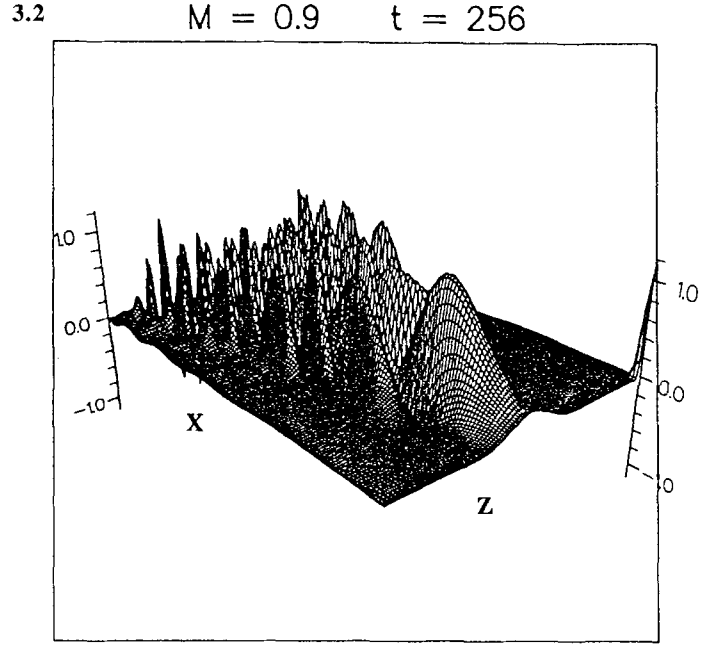

Fig. 3. Numerical results for subsonic range. (See also final page.)
3.1. Contours of disturbance amplitude at large time for $M = 0.9$.
3.2. Surface plot at $M = 0.9$ for large time.
3.3. Intermediate time ($T = 16$) results for $M = 0.9$.
3.4. Results for same time, but $M = 0.98$.
The nearly planar waves predicted by theory are clearly evident, as is their persistence after the centreline waves die out.
3.5. Surface plot (for $\bar{Z} > 0$) showing persistence of plane waves at $M = 0.98$, $T = 16$.
3.6. Comparison of centreline amplitude for $M = 0.9$, $M = 0.98$ at $T = 16$. Note very rapid initial growth at higher Mach number, but more rapid subsequent decay.

for $\chi \equiv \tan \phi$. Potentially there are four main waves possible downstream now rather than just two as in Section 3(iii); see also (4.15a–c) later. We observe also that the solutions near the edges of the wake(s) downstream are still described by an Airy function, as in Section 3(iii), and the ultimate downstream decay at large times T is associated with larger distances, of order T, similarly to Section 3(iii), at general Mach numbers in the subsonic or supersonic range.

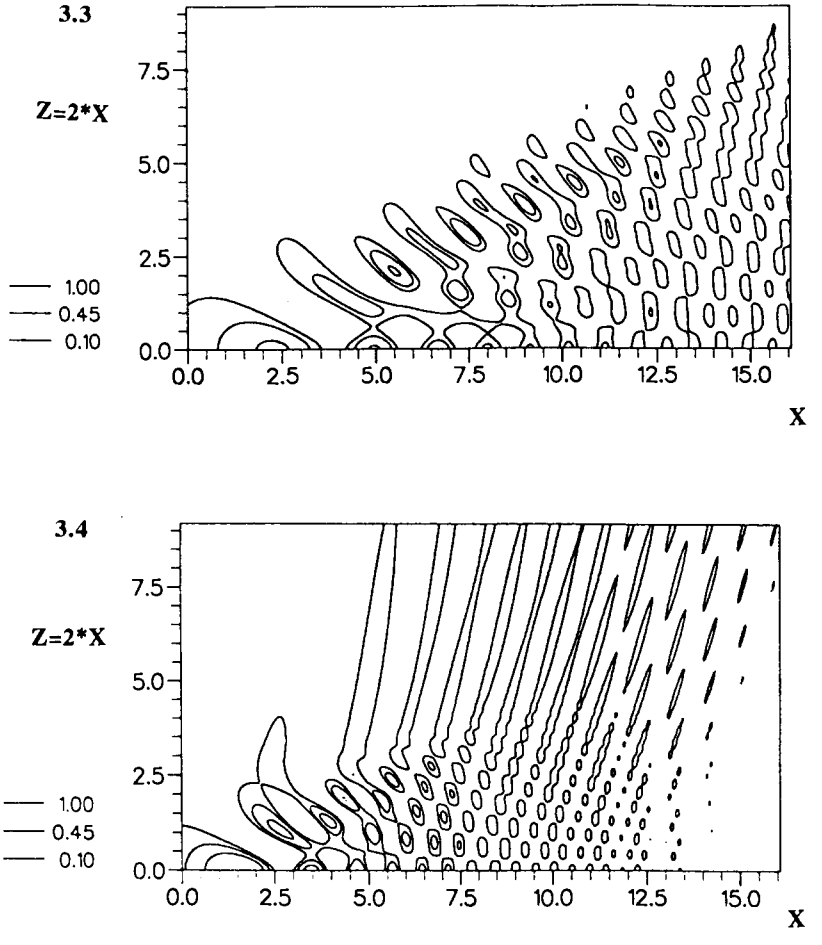

Fig. 3 (cont.).

Two special limits are of most interest next. First, in the *incompressible* limit $M_\infty \to 0$, $\kappa \to 1+$, only two waves remain since (4.4) then yields only two real roots $\chi = \{1 \pm (1 - 8\tan^2\theta)^{1/2}\}/(2\tan\theta)$, the other two roots being imaginary, $\chi = \pm i$. The two real roots here confirm the results in Section 3(iii) and in particular the half-wake angle of $\tan^{-1}(8^{-1/2}) = 19.47°$. Second, in the *transonic* limit $M_\infty \to 1-$, $\kappa \to \infty$, there can be four real roots, three of which are governed by

$$\chi^3 \tan\theta - \chi^2 + 3\chi \tan\theta + 1 = 0 \tag{4.5}$$

with χ of $O(1)$, when θ is $O(1)$, whereas the fourth root has $|\chi| \ll 1$, from (4.4). One root of (4.5) is negative and persists for all angles θ, starting at $\chi = -1$ for zero θ, then increasing monotonically with θ and tending to zero from below as $\theta \to \pi/2$. The other two, positive, roots of (4.5) start at $\chi = 1, \infty$ in effect for $\theta = 0$, then increase/decrease with θ respectively and coalesce at $\chi = 6\tan\theta_c/(1 - 9\tan^2\theta_c)$ for $\theta = \theta_c$, thereafter becoming irrelevant (complex) for $\theta > \theta_c$, where

$$\theta_c = \tan^{-1}[(9 + 6\sqrt{3})^{-1/2}] = 12.79° \tag{4.6}$$

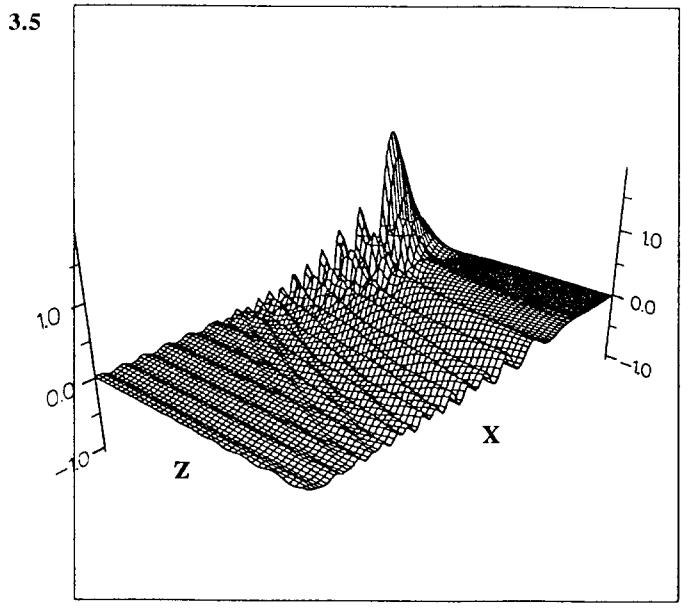

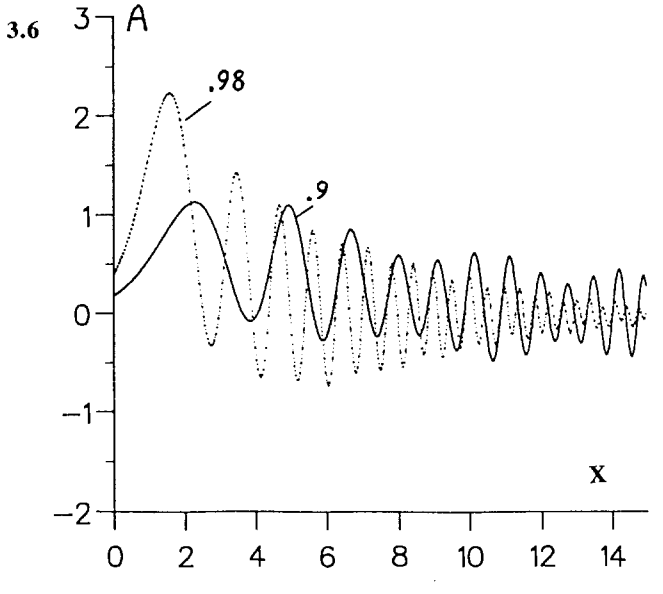

Fig. 3 (cont.).

defines a cut-off angle. Further, at sufficiently large angles $\theta \sim \pi/2 - O(\kappa^{-1})$ the negative root from (4.5) and the fourth root mentioned above become comparable and are associated with a distinct structure in which $\tan\theta \sim \kappa b$, $\chi \sim \kappa^{-1}\tilde{\chi}$ typically, with b, $\tilde{\chi}$ of order unity. Then (4.4) gives a quadratic equation for $\tilde{\chi}$, yielding the two roots

$$\tilde{\chi} = [-1 \pm \{1 - 24b^2\}^{1/2}]/(6b) \tag{4.7a}$$

and hence the second cut-off criterion

$$\theta \sim \frac{\pi}{2} - (24)^{1/2}\kappa^{-1} . \tag{4.7b}$$

Thus the roots (4.7a) correspond to wide waves, of quasi-planar form. An additional feature here, however, concerns the wave amplitudes. The roots in (4.5) correspond to the scalings

$$(\alpha, \beta) = \kappa^{1/2}(\alpha^*, \beta^*) , \qquad (X, Z) = \kappa^{-1/2}(X^*, Z^*) , \tag{4.8a,b}$$

effectively, thereby altering the right-hand side in (4.2) to the form

$$\kappa \int\int \exp\{i\alpha^* X^* + i\beta^* Z^* - i\alpha^*(\alpha^{*2} + \beta^{*2})T/\beta^*\} \, d\alpha^* \, d\beta^* , \tag{4.8c}$$

apart from the Q factor. In consequence, although the associated downstream solution has increased amplitude of order κ, it decays fast spatially, in length scales reduced by $O(\kappa^{-1/2})$. By contrast, the roots in (4.7a) point to the scalings

$$(\alpha, \beta) = (\alpha, \kappa^{-1}\tilde{\beta}) , \qquad (X, Z) = (X, \kappa\tilde{Z}) , \tag{4.9a,b}$$

reducing the right-hand side of (4.2) to

$$\kappa^{-1} \int\int \exp\left\{i\alpha X + i\tilde{\beta}\tilde{Z} - \frac{i\alpha^3 T}{(\alpha^2 + \tilde{\beta}^2)^{1/2}}\right\} d\alpha \, d\tilde{\beta} , \tag{4.9c}$$

except for effects due to Q. Hence this contribution to the downstream response starts with less amplitude, of order κ^{-1}, but then lasts longer since the X-scale stays at $O(1)$. Here (4.8c), (4.9c), when subjected to analysis as in (4.3a,b)ff, can be shown to produce the root equations (4.5), (4.7a), in turn, as expected. More significantly, all the above transonic-flow features, namely (4.6), (4.8a–c) for the *finite-angle waves*, and (4.7b), (4.9a–c) for the *wide quasi-planar waves*, are closely in keeping with the computational results of Fig. 3 at Mach numbers near unity. The relatively rapid spatial decay of the finite-angle contributions, compared with the slow spatial decay of the initially smaller quasi-planar contributions, is particularly noticeable.

In the *supersonic* regime, (4.1b) applies and so, in (4.2),

$$(\alpha^2 + \kappa^2\beta^2)^{1/2} \text{ is replaced by } (\kappa_1^2\beta^2 - \alpha^2)^{1/2} , \tag{4.10}$$

with $\kappa_1 \equiv (M_\infty^2 - 1)^{-1/2}$ ranging from 0 to ∞, and the integration domain is restricted to $|\alpha| < \kappa_1|\beta|$. Again, we obtained computational solutions of (4.2) with (4.10) at several supersonic Mach numbers, as shown in Fig. 4. The analytical working for large times and distances is similar to that for the subsonic case except that now

$$K(\phi) = (\kappa_1^2 \sin^2\phi - \cos^2\phi)^{1/2} \tag{4.11}$$

and hence (4.4) is replaced by

$$\kappa_1^2\chi^4 \tan\theta - \kappa_1^2\chi^3 + 3\kappa_1^2\chi^2 \tan\theta + (\kappa_1^2 + 2)\chi - 2\tan\theta = 0 . \tag{4.12}$$

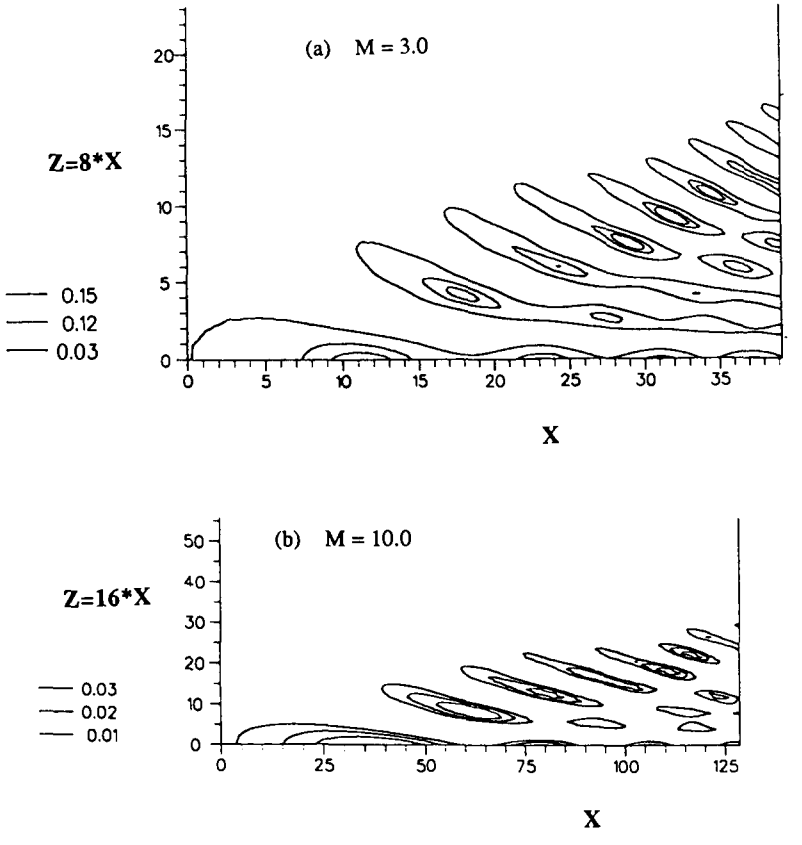

Fig. 4. Numerical results for supersonic range. (See also final page.) (a) $M = 3.0$. (b) $M = 10.0$. The results are similar to those at low Mach numbers but are confined in a very narrow wake.

The *transonic* limit, as $M_\infty \to 1+$, $\kappa_1 \to \infty$, is therefore broadly the same as for $M_\infty \to 1-$, in (4.5)–(4.9c). The *hypersonic limit*, on the other hand, is associated mainly with small angles of spreading downstream. Here $M_\infty \gg 1$, $\kappa_1 \to 0$, and the dominant effects are confined to the interval where $\theta = \kappa_1 \bar{\theta}$, $\chi = \kappa_1^{-1} \bar{\chi}$ with $\bar{\theta}$, $\bar{\chi}$ of $O(1)$. So from (4.12) the governing equation for the four roots present reduces to

$$\bar{\chi}^4 \bar{\theta} - \bar{\chi}^3 + 2\bar{\chi} = 0 . \tag{4.13}$$

For small $\bar{\theta}$ the four roots are at $\bar{\chi} = \pm 2^{1/2}$, 0, $+\infty$ in effect. Their behaviour for increasing $\bar{\theta}$ is then analogous with that in the previous transonic-flow analysis, and in particular a double root and consequent cut-off arise at $\bar{\chi} = 6^{1/2}$ for $\bar{\theta} = 3^{-3/2} 2^{1/2}$, i.e. for the small angle

$$\theta = \theta_c \sim 3^{-3/2} 2^{1/2} M_\infty^{-1} . \tag{4.14a}$$

Concerning the hypersonic amplitudes provoked, the scalings involved now have

$$(\alpha, \beta, X, Z) = O(\kappa_1, 1, \kappa_1^{-1}, 1) . \tag{4.14b}$$

As a result, the typical amplitude is reduced by a factor $\kappa_1 (\sim M_\infty^{-1})$, from (4.2), but the

typical wake length of the spot increases by a factor $\kappa_1^{-1}(\sim M_\infty)$, at least in terms of the present coordinates. The analytical properties above again agree well with the computations (Fig. 4). Indeed, all the different decay rates summarized in (4.8b), (4.9b), (4.14b) are evident numerically in Figs 3 and 4 with the long scale (4.14b) for the hypersonic regime being particular clear in Fig. 4.

There are two final points of interest here, the first of which concerns the spot response near the line of symmetry, where $\theta \to 0$. In the subsonic range (4.4) gives the two roots

$$\chi = \pm(1 - 2\kappa^{-2})^{1/2}, \tag{4.15a}$$

apart from those at small and large χ. Hence the crossover from two to four waves downstream occurs at the subsonic Mach number

$$M_\infty = 2^{-1/2}. \tag{4.15b}$$

(Dr R.I. Bowles, private communication 1991, has kindly pointed out to us that at the crossover value (4.15b) the spanwise group velocity becomes negative, opposite in sign to the spanwise velocity.) The four-wave description also continues throughout the supersonic range, with the two finite-χ roots been given by

$$\chi = \pm(1 + 2\kappa_1^{-2})^{1/2}, \tag{4.15c}$$

from (4.12). These are continuous with the roots (4.15a) in the transonic limit, both sets then agreeing with the limiting result (4.5). Second, the scales quoted in (4.8), (4.9), (4.14b) hold outside the edge layers that arise near the caustics. In contrast, the amplitude maxima tend to occur inside these layers, cf. (3.9). For the transonic limit for instance the maximum amplitude is found to increase like $\kappa^{5/6}T^{1/3}$, being attained where X is $O(\kappa^{-1}T)$, for the contributions corresponding to (4.8), whereas the edge-layer maximum corresponding to (4.9) decreases like $\kappa^{-1}T^{1/3}$, being attained at $X = O(T)$. Likewise, the hypersonic limit can be analyzed for its edge-layer response, yielding a maximum amplitude which decreases as $\kappa_1^{4/3}T^{1/3}$ and is reached at distances X of order T. These results again are in good agreement with the computations of Figs 3 and 4.

5. Further comments

An investigation into initial-value problems for spots in incompressible or compressible boundary layers has been presented above. Figure 5 summarizes the complete Mach-number range, as regards the wake half-angles computed far downstream, and, as with other quantities, there is good agreement with the analysis. The results, throughout Sections 3 and 4, are felt to be of potential practical value in characterizing the downstream progress of spots after an initial disturbance to the boundary layer. The theory developed so far would not necessarily be expected to be applicable directly to previously computed or experimentally observed spots, at least not until nonlinearity is incorporated (see below), but there is some measure of agreement nevertheless. The main analytical prediction in the incompressible case concerns the concentrated wake effect inside a wedge of half-angle 19.47° downstream (as for Kelvin's ship wake, see Section 1), with the maximum disturbance

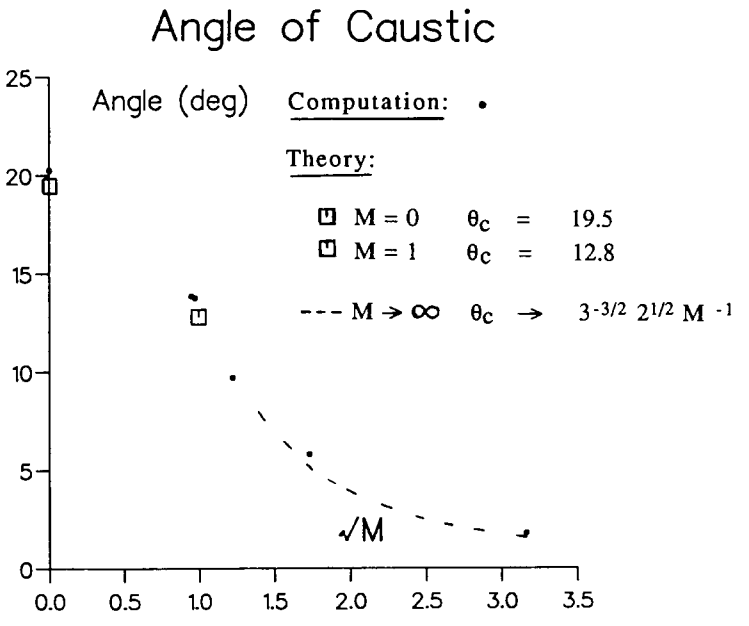

Fig. 5. Summary. Wake half-angle versus Mach number, including comparison between theory and computation.

amplitude occurring near the edges of the wake and with multiple waves in-between. Comparisons between this theoretical response and computational results for the 3D triple-deck problem (see Section 2) are presented by Smith (1987a) and are fairly affirmative; see also Duck (1987), Ryzhov (1987). Comparisons with Gaster & Grant's (1975) laminar-spot experiments are also quite encouraging (Smith 1987a), including the accentuated edge effects downstream at relatively large times, even though in these comparisons and those mentioned in the previous sentence the theory tends to over-estimate the half-angle downstream. Concerning transitional and turbulent spots, there is some additional encouragement both from the general 3D structure (Sections 3 and 4) with multiple waves present downstream, suggesting the study of nonlinear effects there, and from Glezer et al.'s (1989) experimental study focussing on effects near, and just trailing, the edges of spots. In the compressible case, the most interesting features found in the spot development are the changes in the flow scales, structure, and disturbance amplitude, as well as in the wake half-angle, as the Mach number increases [these changes are apart from other factors due to the scalings leading to (2.3) with (4.1), e.g. see Smith 1989]. This is especially so for the transonic and hypersonic ranges, as Section 4 above shows, e.g. with the transonic range producing two spatially distinct kinds of amplitude response downstream, while in the hypersonic range the wake-spreading angle tends to zero.

There are many other areas of possible applications. The influence of cross-flow in the original boundary layer can be incorporated similarly to compressibility effects in Section 4, i.e. by alteration of the pressure-displacement interaction law as in Smith & Stewart (1987b). Channel flows, jets, liquid-layer flows, in certain regimes, and other flows with other interaction laws all require study, as do shorter-scale Rayleigh wave contributions in the incompressible or compressible boundary layer (e.g. Mack 1984, Malik 1987, Brown & Smith 1990) and non-aerodynamic flows. In channel flows, for example, the corresponding wake half-angle is increased to 30°. Spot-disturbance experiments in channel flows, with reduced initial amplitudes, could be of much interest.

Several other applications and consequences suggest themselves, but the nonlinear aspects within the context of Section 2 seem most worthy of emphasis. Among these, there are the 3D nonlinear vortex structures pointed out by Smith (1987b); the wall-sublayer and micro-scales within the Euler stage (SDR); the possibility of small-scale vortex-wave interactions within the present scales; short- or long-scale effects in the spanwise direction; and the eventual occurrence of interactive break-up during sublayer eruption near the wall (Smith 1988, Peridier et al. 1991), as mentioned in Section 1. The most immediate impact of nonlinearity, however, can be seen in the downstream asymptotes of Section 3, for the incompressible regime, and in particular in the finding that the maximum disturbance amplitude occurs in comparatively thin edge-regions. One would therefore expect nonlinear effects to become important first in the edge-regions, rather than in the middle part of the far-wake. Here, as a guide for a subsequent nonlinear study, we note the following. In the edge region, if

$$A \propto T^{-1/2}(XT^{-1/2})^N \tilde{A}(\eta) + \cdots \quad \text{at large } X, T \text{ (with } T^{1/2} \ll X \ll T) \tag{5.1}$$

(cf. (3.9)), approximately, with corresponding expansions for the other flow variables in (2.3), (2.5), and appropriately scaled co-ordinates, then substitution into the latter nonlinear equations leads eventually to an Airy equation for $\tilde{A}(\eta)$, exactly consistent with the form (3.9) as expected, provided that the displacement in (5.1) is sufficiently small, specifically $N < N_0$ for some critical value N_0. If $N = N_0$, however, nonlinear terms enter to alter the governing equation. A similar estimate applies to the compressible regime of Section 4. Research on these matters is in progress, by F.T.S., who suggests that N_0 can equal $\frac{1}{3}$ or zero depending on the flow conditions. It can be shown further that the asymptote (3.9) and its counterpart (5.1) in the nonlinear case hold also for the full Euler system (2.1), such that at large times (t) there are in effect two main areas of activity in the spot, namely at distances of orders $t^{1/2}$ and t downstream, just as in Fig. 2.

Thanks are due to AFOSR (grant no. 89-0475) from F.T.S. and SERC from D.J.D. for support of this and related work.

References

Brown, S.N. and Smith, F.T., The inviscid instability of a Blasius boundary layer at large values of the Mach number. *J. Fluid Mech.* 219 (1990) 499–518.

Cheng, H.K. and Johnson, E.R., Inertial waves above an obstacle in an unbounded, rapidly rotating fluid. *Proc. Roy. Soc.* A 383 (1982) 71–87.

Duck, P.W., private communication (1987).

Gaster, M. and Grant, I., An experimental investigation of the formation and development of a wave packet in a laminar boundary layer. *Proc. Roy. Soc.* A 347 (1975) 253–269.

Gaster, M., A theoretical model of a wave packet in the boundary layer on a flat plate. *Proc. Roy. Soc.* A 347 (1975) 271–289.

Gaster, M., The nonlinear phase of wave growth leading to chaos and breakdown to turbulence in a boundary layer as an example of an open system. *Proc. Roy. Soc.* A 430 (1990) 3–24.

Glezer, A., Katz, Y. and Wygnanski, I., On the breakdown of the wave packet trailing a turbulent spot in a laminar boundary layer. *J. Fluid Mech.* 198 (1989) 1–26.

Hoyle, J.M., Smith, F.T. and Walker, J.D.A., On sublayer eruption and vortex formation. *Comp. Phys. Commns.* 65 (1991) 151–157.

Katz, Y., Seifert, A. and Wygnanski, I., On the evolution of the turbulent spot in a laminar boundary layer with a favourable pressure gradient. *J. Fluid Mech.* 221 (1990) 1–22.

Mack, L.M., Boundary-layer linear stability theory. AGARD, Report 709 (1984).

Malik, M.R., Prediction and control of transition in hypersonic boundary layers. A.I.A.A. paper no. 87-1414 (1987).

Peridier, V.J., Smith F.T. and Walker, J.D.A., Vortex-induced boundary-layer separation. Part 1: the unsteady limit problem $\mathrm{Re}\to\infty$. Part 2: unsteady interacting boundary-layer theory. *J. Fluid Mech.* 232 (1991) 99–131 & 133–165.

Riley, J.J. and Gad-el-Hak, M., In S.H. Davis and J.L. Lumley (eds), *Frontiers in Fluid Mechanics*. Springer-Verlag (1985).

Rothmayer, A.P. and Smith, F.T., Strongly nonlinear wave-packets in boundary layers. *Trans. A.S.M.E., Forum on Unsteady Flow Separation, Cincinnati, Ohio, June 1987*, 52 (1987) 67–79.

Ryzhov, O.S., private communication (1987).

Smith, F.T., Theoretical aspects of steady and unsteady laminar separation. *A.I.A.A. 17th Fluid Dyn., Plasma Dyn. & Lasers Conf.*, 1984 (1984).

Smith, F.T., Theory and computations of 3D steady and unsteady interactive boundary layers. *R.T. Davis Mem. Symp., Cincinnati, Ohio, June 1987* (1987a) in press, *Computers & Fluids* (1991).

Smith, F.T., Break-up in unsteady separation. *Trans. A.S.M.E., Forum on Unsteady Flow Separation, Cincinnati, Ohio, June 1987*, 52 (1987b) 55–64.

Smith, F.T., Finite-time break-up can occur in any unsteady interacting boundary layer. *Mathematika* 35 (1988) 256–273.

Smith, F.T., On the first-mode instability in subsonic, supersonic or hypersonic boundary layers. *J. Fluid Mech.* 198 (1989) 127–153.

Smith, F.T. and Burggraf, O.R. (SB), On the development of large-sized short-scaled disturbances in boundary layers. *Proc. Roy. Soc.* A 399 (1985) 25–35.

Smith, F.T., Doorly, D.J. and Rothmayer, A.P. (SDR), On displacement-thickness, wall-layer and mid-flow scales in turbulent boundary layers, and slugs of vorticity in pipes and channels. *Proc. Roy. Soc.* A 428 (1990) 255–281.

Smith, F.T. and Stewart, P.A., The resonant-triad nonlinear interaction in boundary-layer transition. *J. Fluid Mech.* 179 (1987a) 227–252.

Smith, F.T. and Stewart, P.A., Three-dimensional instabilities in steady and unsteady nonparallel boundary layers, including effects of Tollmien–Schlichting disturbances and cross-flow. *Proc. Roy. Soc.* A 409 (1987b) 229–248.

Walker, J.D.A. and Smith, C.R., Theme Issue on Turbulent Flow. *Trans. Roy. Soc.* A, in press (1991).

Whitham, G.B., *Linear and Nonlinear Waves*. Wiley-Interscience (1974).

Computational results

Using the transformation

$$(X, Z) = T^{1/2}(\bar{X}, \bar{Z}),$$

$$(\alpha, \beta) = T^{-1/2}(\bar{\alpha}, \bar{\beta}),$$

the computational results show $T \cdot \hat{A}(\bar{X}, \bar{Z}, T)$, with $Q(\bar{\alpha}, \bar{\beta}, T) = \exp[-(\bar{\alpha}^2 + \bar{\beta}^2)/16 \cdot T]$, for various values of time, T, and Mach number M, in Figs 1, 3, 4.